Article

Discovery Medicine 2026; 38(206): 695–714
https://doi.org/10.24976/Discov.Med.202638206.58

Integrated DNA Methylation and Transcriptomic Analysis Under Microgravity Reveals the Dnmt3a–Ddit3 Axis Regulating Osteoblast Apoptosis

Chongxiao Sun[1], Fei Teng[1], Yayi Xia[1,*]

[1]Department of Orthopaedics, Orthopaedics Clinical Medicine Research Center of Gansu Province, Intelligent Orthopedics Industry Technology Center of Gansu Province, Lanzhou University Second Hospital, 730030 Lanzhou, Gansu, China
*Correspondence: xiayayi2025@163.com (Yayi Xia)
Submitted: 27 December 2025 Revised: 9 January 2026 Accepted: 28 January 2026 Published: 20 March 2026

Background: Osteoporosis is a systemic skeletal disease with a multifactorial pathogenesis, and microgravity contributes significantly to its progression. Despite the critical role of epigenetic modifications, particularly DNA methylation, in cellular function, their involvement in microgravity-induced osteoporosis remains unclear. This study investigates the impact of DNA methylation on osteoblast phenotypes under microgravity, offering new insights into the epigenetic regulation of bone homeostasis.

Methods: Reduced representation bisulfite sequencing (RRBS), methylation-specific PCR (MSP), bisulfite sequencing PCR (BSP), and quantitative PCR (qPCR) were used to analyze the DNA methylation and transcriptional profiles of MC3T3-E1 cells under microgravity. Differentially methylated regions (DMRs) in the Ddit3 promoter and its expression were assessed. Functional assays, including Western blotting (WB), flow cytometry, and CCK-8, were performed to evaluate the impact of Dnmt3a overexpression or Ddit3 inhibition on osteoblast function. *In vivo*, a tail suspension (TS) mouse model was used to investigate bone phenotypic changes after Ddit3 inhibition. The role of the endoplasmic reticulum (ER) stress pathway in mediating Ddit3's effects was examined using the ER stress inhibitor 4-phenylbutyric acid (4PBA).

Results: Microgravity exposure markedly induced apoptosis in osteoblasts, with the apoptotic rate increasing from 3.83% in the control group to 13.44% in the microgravity group ($p < 0.05$). Pro-apoptotic proteins Bax and cleaved caspase-3 increased by 30% ($p < 0.05$) and 66% ($p < 0.05$), respectively, whereas the anti-apoptotic protein Bcl-2 decreased by 33% ($p < 0.05$). Reduced representation bisulfite sequencing (RRBS) revealed a significant global decrease in DNA methylation under microgravity. RT-qPCR analysis demonstrated a 48% reduction in Dnmt3a expression ($p < 0.05$), accompanied by hypomethylation of the Ddit3 promoter and a 2.36-fold elevation of Ddit3 mRNA ($p < 0.05$). BSP further confirmed a 62% ($p < 0.05$) decrease in Ddit3 promoter methylation, while MSP showed a 45% reduction ($p < 0.05$). Functional assays indicated that Dnmt3a overexpression elevated cell viability by 31% ($p < 0.05$) and suppressed apoptosis, reducing Bax expression by 35% ($p < 0.05$) and increasing Bcl-2 expression by 103% ($p < 0.05$) compared with the microgravity group. Moreover, the regulatory effects of Dnmt3a were Ddit3-dependent; inhibition of Ddit3 under microgravity reduced the apoptotic rate by 58% ($p < 0.05$) relative to Dnmt3a-inhibited cells. Microgravity also strongly activated the ER stress pathway, upregulating p-PERK, p-IRE1α, and XBP1s by 3.2-, 2.1-, and 3.8-fold ($p < 0.05$), respectively. Under microgravity, Ddit3 inhibition alleviated ER stress, decreasing p-PERK, p-IRE1α, and XBP1s by 57% ($p < 0.05$), 48% ($p < 0.05$), and 56% ($p < 0.05$), respectively. Furthermore, treatment with the ER stress inhibitor 4PBA under microgravity reduced the ER stress markers ATF4 and XBP1s by 48% ($p < 0.05$) and 49% ($p < 0.05$), respectively. *In vivo* studies using a TS mouse model confirmed that Ddit3 inhibition attenuated the osteoporosis-like phenotype, improving bone mass and microarchitectural integrity.

Conclusion: Under microgravity, Dnmt3a downregulation induces Ddit3 promoter hypomethylation, triggering ER stress and osteoblast apoptosis, thereby promoting osteoporosis. These findings identify the Dnmt3a–Ddit3 axis as a key epigenetic regulator of osteoblast dysfunction in microgravity and a promising therapeutic target for microgravity-induced osteoporosis.

Keywords: microgravity; osteoporosis; Dnmt3a; Ddit3; DNA methylation; osteoblasts; ER stress

Introduction

Osteoporosis arises from multiple contributing factors and is characterized by a decline in bone density and mass due to disruptions in bone microarchitecture. This condition increases bone fragility, making individuals more susceptible to fractures from low-impact forces, commonly referred to as fragility fractures [1]. Such fractures significantly diminish patients' quality of life, heighten morbidity, and, in severe cases, lead to disability or even death [2]. The primary risk factors for osteoporosis include advanced age, low body weight, smoking, a family history of osteoporosis, early menopause, low levels of physical activity, and a personal history of fractures from minor trauma or ground-level falls. These factors collectively accelerate bone loss [3]. Additionally, certain medical conditions such as hyperparathyroidism, anorexia nervosa, malabsorption, hyperthyroidism, overt thyrotoxicosis, and chronic kidney disease can predispose individuals to osteoporosis [4].

Furthermore, osteoporosis is a metabolic bone disorder arising from an imbalance between osteoclasts' bone-resorbing activity and osteoblasts' bone-forming activity. This imbalance leads to progressive loss of bone mass and strength, increasing the risk of fragility fractures and impairing the healing process after fractures [5,6]. The global incidence of osteoporotic fractures, particularly hip, vertebral, and wrist fractures, continues to rise, establishing osteoporosis as a critical public health issue worldwide [7].

The pathogenesis of osteoporosis involves both genetic determinants and hormonally regulated endogenous factors, while environmental changes serve as significant exogenous contributors [8]. Studies have shown that astronauts are at risk of losing 1.0% to 1.5% of their bone mass per month while in space, and upon returning to Earth, they are unable to fully recover their bone mass, leaving them more vulnerable to osteoporosis. This bone loss is primarily attributed to the impairment of osteoblast function due to microgravity, followed by upregulation of osteoclast-mediated bone resorption [9]. Therefore, changes in the mechanical environment of bone tissue—such as under conditions of weightlessness or hypergravity—disrupts the equilibrium of bone cell physiology, leading to metabolic abnormalities in bone and the development of related diseases. Specifically, these changes can affect osteoblast proliferation and apoptosis [10], with osteoblast apoptosis playing a key role in the onset of osteoporosis [11]. Previous research has demonstrated that glucocorticoids promote osteoporosis by inducing osteoblast apoptosis, thereby reducing the number of bone cells [12]. This underscores the importance of reversing osteoblast apoptosis as a therapeutic strategy for osteoporosis. Therefore, investigating whether osteoblasts undergo apoptosis and understanding the underlying biological mechanisms in the context of weightlessness is essential for developing new treatment approaches.

Research has shown that epigenetic regulation plays a significant role in bone metabolism and the imbalance of age-related bone homeostasis [13,14]. It has also been reported that microgravity can substantially affect the osteogenic differentiation capacity of stem cells through epigenetic modifications [15]. Among these modifications, abnormal DNA methylation is a key factor in the development of osteoporosis [16]. DNA methylation refers to the covalent attachment of a methyl group to the 5′ carbon of cytosine in CpG dinucleotides, a process catalyzed by DNA methyltransferases, which regulates gene transcription and is involved in cellular function control [17]. Dnmt3a is a critical enzyme that mediates DNA methylation modifications. Recent studies have emphasized the importance of Dnmt3a in various biological processes, including development, differentiation, and disease [18,19]. A comparative transcriptomic analysis has identified Dnmt3a as being linked to osteoporosis [20]. In osteoblast regulation, Dnmt3a has been shown to promote osteoblast differentiation and alleviate osteoporosis [21]. Additionally, Dnmt3a has significant anti-apoptotic effects in ovarian, cervical, and pancreatic cancer cells [22–24]. Interestingly, previous studies have found that microgravity can significantly influence the dynamic expression of Dnmt3a [25]. However, it remains unclear how microgravity affects Dnmt3a expression in bone tissue, and whether it can modulate osteoblast apoptosis to contribute to osteoporosis development.

In this study, we found that abnormal DNA methylation-induced upregulation of Ddit3 is associated with osteoporosis. Further experiments demonstrated that in a microgravity-induced osteoporotic mouse model, intervening with Ddit3 by inhibiting osteoblast apoptosis caused by ER stress effectively protected against osteoporosis. These findings reveal an important epigenetic mechanism in the development of osteoporosis under microgravity conditions and offer potential therapeutic strategies to reduce bone loss in astronauts and individuals exposed to similar conditions on Earth.

Methods

Reagents

Minimum Essential Medium α (MEM α; 12561056), phosphate-buffered saline (PBS) (10010023), 0.25% Trypsin-EDTA (25200), penicillin/streptomycin (P/S) (15140122) and fetal bovine serum (FBS) (16000044) were purchased from Gibco (Gaithersburg, MD, USA). Dnmt3a (A3169), Bax (A19684), Bcl-2 (A20736), Cleaved-Caspase-3 (A22869), and GAPDH (AC002) antibodies were purchased from ABclonal (Wuhan, China). The p-IRE1α (Invitrogen, PA1-16927) was purchased from Invitrogen (Waltham, Massachusetts, USA). The p-PERK antibody (3179T) was purchased from Cell Signaling Technology (CST) (Danvers, MA, USA). The OCN antibody (GB11233) was purchased from Servicebio (Wuhan, China). Anti-mouse (A0216) or Anti-rabbit HRP-

conjugated secondary antibodies (A0208) were purchased from Beyotime (Beijing, China). The transfection reagent Lipofectamine 3000 (L3000150) was purchased from Invitrogen (Waltham, Massachusetts, USA). 4-Phenylbutyric acid (4PBA) (HY-A0281), an ER stress inhibitor, was purchased from MedChemExpress (MCE) (Monmouth Junction, NJ, USA).

Cell Culture and Treatment

For this study, mouse pre-osteoblastic cell line MC3T3-E1 (RRID: CVCL_0409) ordered from Shanghai Fuheng Biotechnology Co., Ltd. (Cat No. FH0384) in February 2024 were used. All cell lines were routinely tested and were negative for mycoplasma contamination. The MC3T3-E1 cell line was authenticated by STR profiling (ABI 3730XL analyzer). MC3T3-E1 cells were maintained in MEM α supplemented with 10% FBS and 1% P/S at 37 °C in a 5% CO_2 atmosphere with 95% humidity. The microgravity cell model was established by using rotation to simulate the microgravity environment, employing a Rotating Cell Culture System (RCCS, Synthecon Inc). The culture of MC3T3-E1 cells under simulated microgravity was achieved by implementing modifications to previously reported methodologies [26]. Briefly, Cytodex 3 microcarriers were used as cell media. Cells with 80%–90% confluence were selected, digested with trypsin, resuspended, and counted. In the simulated microgravity group, 5×10^4 cells were mixed with microcarriers, and the cell-microcarrier mixture was added to the culture dish. After removing air bubbles, the dish was placed into the RCCS device, set to a rotation speed of 15 rpm/min, and cultured for 48 hours at 37 °C with 5% CO_2. The detailed procedure is illustrated in **Supplementary Fig. 1**. All conditions for the normal gravity group remain the same except for the rotation. According to the experimental design, cells from each group were to be used for subsequent phenotype or molecular function validation. Cells were transfected with pcDNA3.1-Dnmt3a (OE-Dnmt3a) to upregulate Dnmt3a expression, with the pcDNA3.1 empty vector serving as the negative control. For gene silencing, specific siRNAs targeting Dnmt3a and Ddit3 were used, and a non-targeting siRNA (SiNC) served as the negative control. All plasmid vectors and siRNAs were purchased from GenePharma (Shanghai, China). Specific experimental manipulations are outlined below. Briefly, cells were cultured in a 12-well plate. According to the Lipofectamine 3000 transfection reagent (Invitrogen) protocol for plasmid and siRNA transfection, 1 µL of plasmid (1 µg/µL) or siRNA (25 nM) was mixed with Lipofectamine 3000 transfection reagent and incubated for 15 minutes. Then, the mixture was added to the wells of the 12-well plate and incubated for 24 hours. Cells were pretreated with DMSO or 4PBA at the designated concentration (5 mM) and duration as required. For siRNA sequences, see **Supplementary Table 1**.

Quantitative Real-Time PCR (qRT-PCR) Analysis

The total RNA from MC3T3-E1 cells in each group was extracted using the Ultrapure RNA Kit (CWBIO, CW0581S) and reverse-transcribed into cDNA with the SuperRT cDNA Synthesis Kit (CWBIO, CW0741M). qRT-PCR was conducted using the SuperStar Universal SYBR Master Mix (CWBIO, CW3360H) and a CFX96 Real-Time PCR Detection System (Bio-Rad). The primers used are listed in **Supplementary Table 2**.

Western Blot Assay of Protein Expression

Cellular proteins were extracted from different experimental groups using RIPA buffer (Beyotime, P0013B). Proteins were separated via SDS-PAGE and transferred to PVDF membrane (Millipore). The membranes were incubated with primary antibodies specific to Dnmt3a (Abclonal, A3169; 1:1000), Bax (Abclonal, A19684; 1:1000), Bcl-2 (ABclonal, A20736; 1:1000), Cleaved-Caspase 3 (ABclonal, A22869; 1:1000), p-IRE1α (Invitrogen, PA1-16927; 1:1000), p-PERK (CST, 3179T; 1:1000), and GAPDH (Abclonal, AC002; 1:5000). The membranes were then incubated with a secondary antibody (Beyotime; 1:2000). Protein bands were visualized using enhanced chemiluminescence (Abclonal, RM00021) and analyzed using Image Lab software (Bio-Rad). After normalization to the intensity of the housekeeping protein (GAPDH), data from each experimental group were compared with those from its corresponding control group, followed by statistical analysis.

Flow Cytometry Analysis of Apoptosis

Cell apoptosis was assessed using the Annexin V-FITC/PI Apoptosis Detection Kit (Cat. No. 40302ES20, Yeasen Biotech, China). Cells were collected and washed twice with PBS. The cell pellet was resuspended in 1× binding buffer and incubated with Annexin V-FITC and PI. After gentle vortexing, the cells were incubated in the dark at room temperature for 15 minutes. Following incubation, 500 µL of 1× binding buffer was added, and apoptosis was analyzed using a Beckman flow cytometer with the corresponding software. Cell components were distinguished using forward and side scatter parameters. Cells positive for Annexin V and negative for PI were defined as early apoptotic, whereas those positive for both Annexin V and PI were classified as late apoptotic. The combined populations in the Q2 and Q3 quadrants were calculated to represent the percentage of apoptotic cells among the analyzed samples.

Cell Proliferation Assay

After culturing cells from each group in a rotating cell culture system in 96-well plates for 12 hours, Dnmt3a expression was modulated or left unchanged for 24 hours, as required by the experimental protocol. Finally, assess-

ment of cell proliferation was carried out using the CCK-8 reagent (Cat. No. 40203ES80, Yeasen Biotech, China).

Reduced Representation Bisulfite Sequencing (RRBS)

In this study, we conducted Reduced Representation Bisulfite Sequencing (RRBS) to analyze the methylation patterns of MC3T3-E1 osteoblast under microgravity and normal culture conditions. Genomic DNA was extracted using the FastPure® Cell/Tissue DNA Isolation Mini Kit (DC102) from Vazyme Biotech Co., Ltd., following the manufacturer's protocols to ensure high-quality DNA suitable for downstream applications. Library construction was performed using the Zymo-Seq RRBS Library Kit (D5460), adhering to a precise workflow designed for optimal results. The process began with the digestion of genomic DNA using the MspI enzyme, which specifically recognizes and cleaves CpG-rich regions, thereby enriching for these important genomic sites. After digestion, cytosine-methylated adapters were ligated to the ends of the fragmented DNA to facilitate subsequent amplification and sequencing. Following adapter ligation, the DNA underwent bisulfite conversion, which converts unmethylated cytosines into uracils. This critical step allows for the differentiation of methylated from unmethylated cytosines during sequencing. The converted DNA was then subjected to index primer amplification to enrich the library and incorporate unique identifiers for multiplexing.

The insert size of the constructed library was analyzed using the Bioanalyzer system (Agilent), ensuring that the fragments were of the desired size for sequencing. The concentration of the library was quantified using the Qubit fluorometer, providing a precise measurement necessary for optimal loading onto the sequencing platform.

Finally, the prepared libraries were sequenced on the Illumina Novoseq 6000 platform with a paired-end read length of 150 base pairs (PE150). The raw RRBS data are available on SRA Bioproject accession PRJNA1192047.

RNA Sequencing

RNA Sequencing (RNA-seq) was further performed to investigate the transcriptomic changes of MC3T3-E1 osteoblasts under microgravity and normal culture conditions. Total RNA was extracted from the cultured cells using the TRIzol reagent (Thermo Fisher Scientific, Cat. No. 15596018) according to the manufacturer's instructions, ensuring the integrity and purity of the RNA for downstream applications.

Library construction was carried out using the NEBNext UltraTM RNA Library Prep Kit (NEB, Cat. No. E7490). The workflow began with the removal of ribosomal RNA (rRNA) to enrich for mRNA, which was followed by fragmentation of the mRNA. The fragmented mRNA was then reverse transcribed into cDNA, and the cDNA underwent end-repair and A-tailing, preparing it for adapter ligation. Adapters containing sequences for sequencing and indexes for multiplexing were ligated to the ends of the cDNA fragments.

Subsequent to adapter ligation, the libraries were purified using the AMPure XP system (Beckman Coulter) to remove any unligated adapters and other contaminants. The quality and size distribution of the constructed libraries were assessed using the Agilent Bioanalyzer system, ensuring that the fragments met the criteria for optimal sequencing. The concentration of each library was quantified using the Qubit fluorometer, yielding precise measurements required for effective loading onto the sequencing platform. Finally, the prepared libraries were sequenced on the Illumina Novaseq 6000 platform, employing a paired-end read length of 150 base pairs (PE150). This sequencing approach allowed for comprehensive coverage of the transcriptome, facilitating the analysis of gene expression profiles under the specified conditions. The raw RNA-seq data are also available on SRA Bioproject accession PRJNA1192047.

Bioinformatic Analysis

Quality control of the raw sequencing data was performed using FastQC and Fastp (or Trim Galore). For RRBS data, we obtained an average of 24.2 million read pairs per sample. The data exhibited high sequencing quality, with Q30 scores consistently exceeding 81% and low duplication rates (<7%). The average mapping efficiency to the reference genome was approximately 69% using Bismark, with a bisulfite conversion rate greater than 96.5%, ensuring reliable methylation calling. For RNA-seq data, an average of 23.6 million clean reads were generated per sample. The transcriptomic data showed exceptional quality (Q30 >95%) and high alignment rates (>98%) to the reference genome using HISAT2. Detailed sequencing statistics for all biological replicates are provided in **Supplementary Table 3**.

For RRBS analysis, raw reads were trimmed using Trim Galore (http://www.bioinformatics.babraham.ac.uk/projects/trim_galore/) to remove adapter sequences and low-quality nucleotides. The trimmed FASTQ files were then aligned to the mm10 reference genome using Bismark [27]. Methylation levels at cytosine sites and within defined small windows (200–1000 bp) were computed using BatMeth2 [28]. Further analysis involved calculating methylation levels across promoter and gene body regions, as well as upstream and downstream areas. Differential methylation analysis was conducted using the MethylKit package to identify differentially methylated cytosines (DMCs) [29], and DMRs. Detected DMRs were filtered according to specific criteria: (1) a p-value less than 0.05; (2) a methylation level difference greater than 0.15; (3) a minimum of 5 CpG sites contained within the DMR; and (4) a DMR length greater than 50 bp. Finally, the Genomation package was utilized for annotating the DMRs to elucidate their functional significance in the genome.

To process the raw RNA-seq data, we began with quality control and trimming of the FASTQ files using TrimGalore. Following this, the cleaned reads were aligned to the mm10 reference genome using HISAT2 (http://daehwankimlab.github.io/hisat2). Subsequently, we utilized StringTie (http://ccb.jhu.edu/software/stringtie/) to quantify the expression levels of mRNAs based on the alignment results. For differential expression analysis, we employed the DESeq2 package to analyze the raw counts matrix. Genes were considered differentially expressed when the adjusted *p*-value (*p*adj) was less than 0.05. To gain insights into the biological significance of the differentially expressed genes, we conducted enrichment analyses using the clusterProfiler package, which provided Gene Ontology (GO) and KEGG pathway enrichment results. Additionally, Gene Set Enrichment Analysis (GSEA) was performed based on the MSigDB database (https://www.gsea-msigdb.org/gsea/msigdb/) to further explore the functional implications of the identified gene sets.

Methylation-Specific PCR (MSP) and Bisulfite-Sequencing PCR (BSP)

To investigate the methylation status of the Ddit3 gene promoter, specific primers were designed using the MetPrimer software (http://www.urogene.org/methprimer). MSP was performed on genomic DNA extracted from MC3T3-E1 osteoblasts cultured under microgravity and normal conditions. Genomic DNA was converted using the Beyotime DNA Bisulfite Conversion Kit (D0068S) before PCR amplification.

For MSP, we utilized the following primers: the methylated forward primer Ddit3-F-M (ATTTCGTTTTTAGAAGGTATCGC) and the reverse primer Ddit3-R-M (CTATTAACTCGCTACTATCCGCT), generating a product of 153 bp with a melting temperature (Tm) of 77.2 °C. The unmethylated forward primer Ddit3-F-U (TTTTGTTTTTAGAAGGTATTGTGT) and the reverse primer Ddit3-R-U (CTCCTATTAACTCACTACTATCCACT) were used, resulting in a product size of 155 bp and a Tm of 72.2 °C.

Additionally, BSP was conducted to further elucidate the methylation patterns of the Ddit3 promoter. The BSP utilized the forward primer (GTTATAGGGGTTAGGGGTAGTTTTG) and reverse primer (AAAATTAATAAAAAATTATAAAAAAAA). Amplified products were purified using a PCR Product Purification Kit (Cat. No. B518141, Sangon Biotech, China) and subsequently cloned into the pGEM-TEasy vector system (Promega, USA). Five colonies from each PCR reaction were randomly selected for sequencing, and the percentage of methylated cytosines relative to total cytosines within the cloned fragments was calculated.

Animal Model and Treatment

This study was conducted in strict accordance with ethical standards for animal experimentation and scientific research. All procedures were approved by the Animal Ethics Committee of The Second Hospital of Lanzhou University (No. D2024-685) and complied with the ARRIVE guidelines (Animal Research: Reporting *In Vivo* Experiments). A total of twenty-four male C57BL/6 mice were used in this study, and all animals were housed and maintained under specific pathogen-free conditions. Male C57BL/6 mice at 4 weeks of age were randomly assigned to two groups: a control group and a tail suspension (TS) group. Mice in the TS group were placed individually in cages and suspended by their tails for 24 hours a day for 7 consecutive days, with a 45-degree downward tilt [30]. Their hindlimbs were in contact with the ground and they had access to food. Following the manufacturer's guidelines (GenePharma, China), we established a mouse model with Ddit3 gene inhibition using Adeno-Associated Virus type 2 (AAV2). AAV2-NC was used as the negative control. C57BL/6 mice were divided into the AAV2-NC normal group, AAV2-NC osteoporosis group, AAV2-Ddit3 normal group, and AAV2-Ddit3 osteoporosis group. The viruses were injected subcutaneously targeting the distal femoral surface at a dose of 2×10^{11} vg/week, two weeks prior to the start of the tail suspension experiment. Mice were euthanatized by cervical dislocation.

Micro-CT Imaging

Mouse femur samples were fixed in 4% buffered formalin for 24 hours and then scanned using a μCT imaging (μCT100 Scanco Medical). The femur specimens were placed on the micro-CT scanning platform with the following settings: tube voltage of 70 kV, tube current of 200 μA, slice thickness of 20 μm, exposure time of 300 ms, and a 360-degree rotation scan. The proximal femur was scanned, and a standard phantom was used for CT calibration. After scanning, a cylindrical region of interest (ROI) with a 2 mm diameter and 1 mm thickness was selected in the center of the femoral neck. Bone tissue within the ROI was analyzed using 3D visualization. Bone mineral density (BMD) was quantified using the Scanco microCT μ100 software, and 3D structural parameters were assessed, including bone volume fraction (BV/TV %), trabecular thickness (Tb.Th), trabecular separation (Tb.Sp), and trabecular number (Tb.N).

Histological and Immunohistochemical (IHC) Staining

The samples were initially fixed in 4% paraformaldehyde for 24 hours, followed by decalcification in a decalcification solution. After decalcification, the samples were washed in distilled water for 48 hours and subjected to dehydration through an ethanol gradient. The samples were then embedded in paraffin and sectioned. Finally, the

sections were stained using H&E and Masson's trichrome staining methods. For IHC staining, tissue sections were incubated overnight at 4 °C with a primary antibody targeting osteocalcin (OCN) (1:200, Cat. No. GB11233; ServiceBio, China), followed by incubation with a secondary antibody conjugated to HRP (1:200, Cat. No. GB23303; ServiceBio, China). The slides were then treated with a DAB horseradish peroxidase substrate kit (Cat. No. P0203, Beyotime Biotech, China) for color development and counterstained with hematoxylin. The staining results were examined under a microscope.

Statistical Analysis

All experiments were independently repeated at least three times. Group comparisons were performed using the independent-samples *t*-test, while multiple comparisons were conducted using one-way ANOVA with GraphPad software (GraphPad Prism 8; GraphPad, Bethesda, MD, USA). For ANOVA, Tukey's post hoc test was applied when normality and homogeneity of variance were satisfied; if assumptions were violated, Welch's ANOVA followed by Dunnett's T3 or the Kruskal-Wallis test followed by Dunn's multiple-comparisons test was used. Continuous variables are expressed as mean ± SD. A *p*-value of less than 0.05 was considered statistically significant.

Results

Microgravity Induces Apoptosis in Osteoblasts

To simulate the microgravity condition and investigate the effects of this environment on the osteoblast phenotype, we used a rotating cell culture system, with a particular focus on whether it could induce cell apoptosis. The morphological characteristics of cells under microgravity conditions are shown in **Supplementary Fig. 2**. We first evaluated the expression levels of osteoblast-specific extracellular matrix genes, *Bglap*, *Runx2*, and *Col1a1*, using quantitative PCR. Under microgravity conditions, the expression of these genes was significantly lower than that observed under normal gravity, with *Bglap*, *Runx2*, and *Col1a1* showing reductions of approximately 45% ($p < 0.001$), 52% ($p < 0.001$), and 57% ($p < 0.001$), respectively. These findings demonstrate that microgravity substantially inhibits osteoblast activity (Fig. 1A). To further evaluate cell proliferation, we performed a CCK-8 assay to examine the effects of microgravity on osteoblast growth. The results revealed that microgravity markedly suppressed cell proliferation, with an approximate 48% reduction ($p < 0.001$) compared with the normal gravity condition (Fig. 1B). Next, cell apoptosis was quantified by flow cytometry. A marked increase in apoptotic rate was observed under microgravity, from 3.83% in the control group to 13.44% in the microgravity group, demonstrating that microgravity substantially enhances osteoblast apoptosis ($p < 0.001$) (Fig. 1C,D). Western blot analysis of key apoptotic proteins further revealed pronounced alterations in apoptosis-related markers in the microgravity-treated group. Specifically, the expression levels of Bax and Cleaved-caspase-3 were increased by approximately 30% ($p < 0.05$) and 66% ($p < 0.05$), respectively, whereas Bcl-2 expression was reduced by about 33% ($p < 0.05$) compared with the control group (Fig. 1E). Together, these findings confirm that microgravity induces osteoblast apoptosis.

Methylation Pattern Analysis

In this study, we analyzed the genomic methylation landscape of our samples. Coverage statistics revealed variation in sequencing depth among chromosomes, with chromosome M showing the highest coverage and chromosome X the lowest. The average genome-wide methylation level was 0.097. Analysis of methylation patterns in different contexts (CpG, CHG, CHH) indicated that CpG sites exhibited markedly higher methylation levels, whereas CHG and CHH sites showed substantially lower levels (Fig. 2A,B). Chromosomal window analysis demonstrated that CpG methylation was enriched in regions with higher gene density, while CHG and CHH methylation remained relatively low (Fig. 2C). Examination of genomic elements revealed that CpG methylation levels were highest within gene bodies and comparatively reduced in upstream and downstream regions, with CHG and CHH methylation remaining consistently low (Fig. 2D).

In the CpG context, we observed a canonical negative correlation between promoter methylation and gene expression levels (Fig. 2E). Specifically, genes with higher expression levels (rank 4 and rank 5) exhibited a pronounced "valley" of hypomethylation around the transcription start site (TSS). This pattern aligns with the established biological concept that promoter hypomethylation facilitates chromatin accessibility and transcription factor binding, thereby actively promoting transcriptional initiation. Conversely, lower expression levels (rank 1–3) were associated with elevated promoter methylation, consistent with the role of DNA methylation in transcriptional silencing. Furthermore, while promoter regions were hypomethylated, gene body regions showed higher methylation levels, which may function to repress spurious transcription initiation from cryptic promoters within the gene body. Regarding non-CpG contexts (CHG and CHH), methylation levels remained minimal and stable across all expression ranks. This observation confirms that non-CpG methylation is rare in differentiated somatic cells like MC3T3-E1, unlike in plants or embryonic stem cells.

Methylation Pattern Changes Under Microgravity Stimulus

We explored the changes in methylation patterns under microgravity stimulus. The methylation levels of CpG, CHG, and CHH in the microgravity group were significantly lower than those in the normal culture group

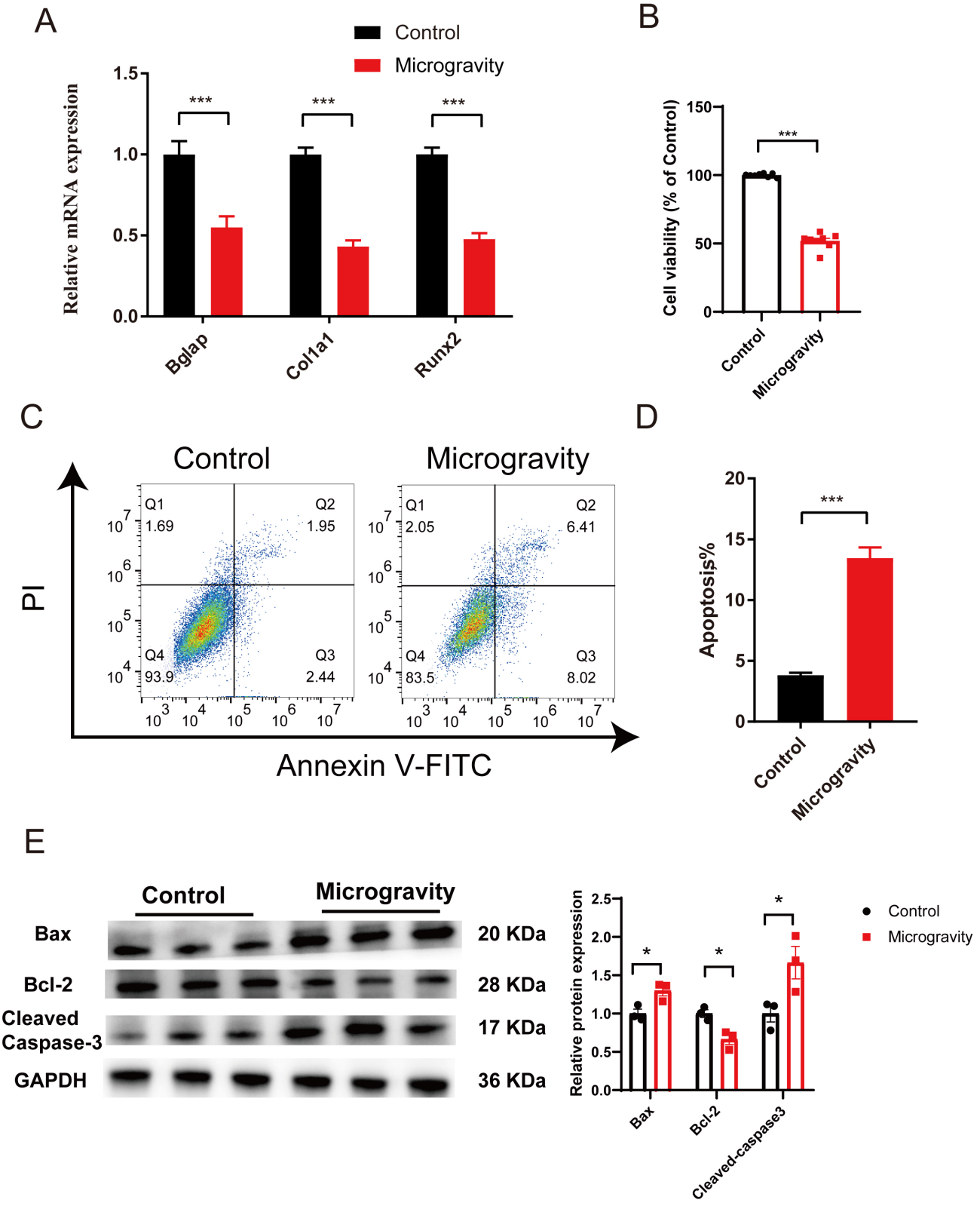

Fig. 1. Effects of microgravity on osteoblast phenotype and apoptosis. (A) PCR analysis of *Bglap*, *Runx2* and *Col1a1* gene expression to assess osteoblast activity. (B) CCK-8 assay to evaluate cell proliferation under microgravity conditions. (C,D) Flow cytometry analysis of apoptosis in osteoblasts under microgravity. (E) Western blot analysis of apoptotic markers (Cleaved-caspase-3, Bax, Bcl-2) in response to microgravity. Data shown as mean ± SD (n ≥ 3), *$p < 0.05$; ***$p < 0.001$.

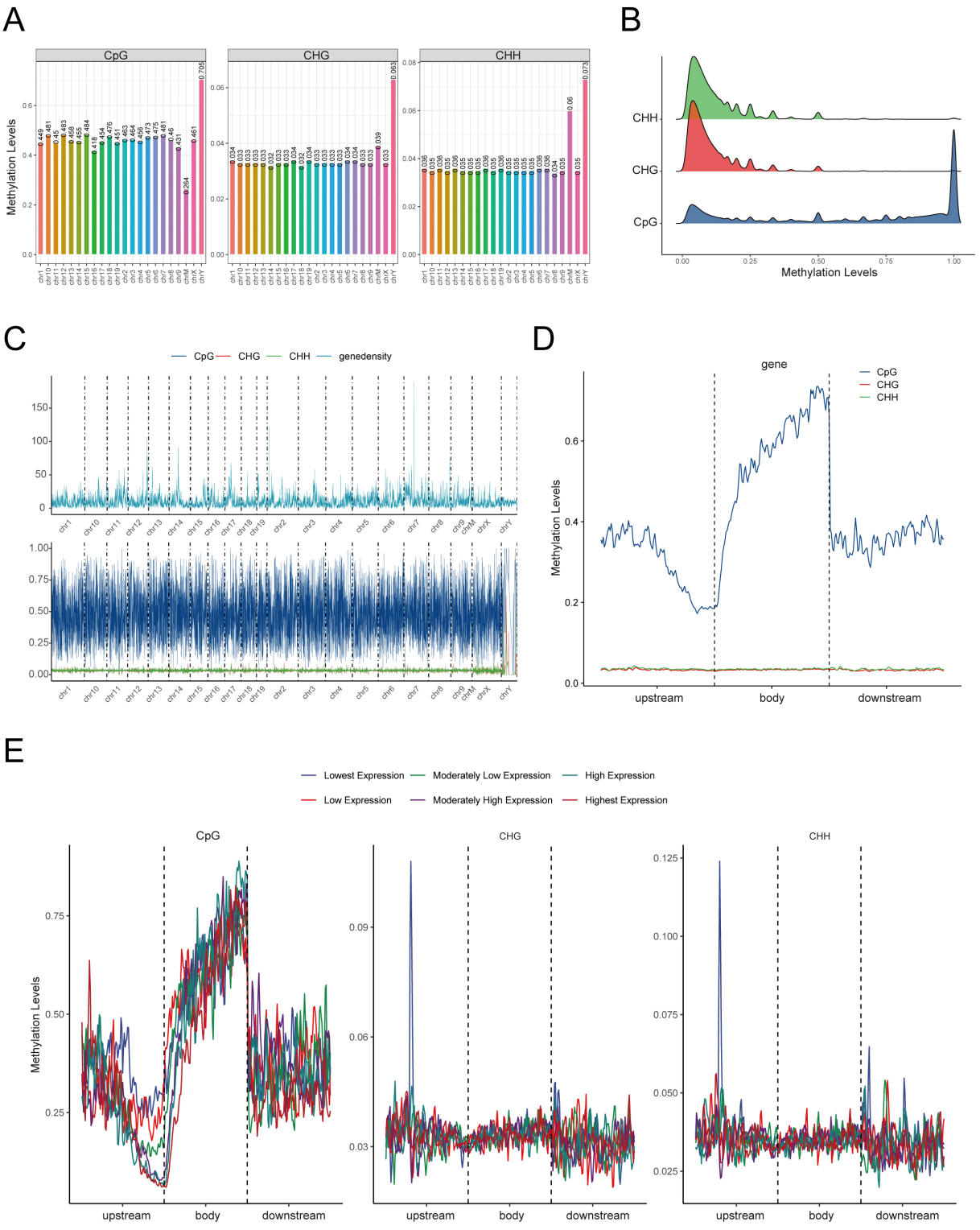

Fig. 2. Genome-wide DNA methylation pattern analysis in MC3T3-E1 cells. (A) Distribution of methylation levels across chromosomes under different sequence contexts (CpG, CHG, and CHH). (B) Distribution density of methylation levels in CpG, CHG, and CHH contexts across the genome. (C) Chromosomal distribution of methylation levels shown in sliding windows. Upper panel shows gene density distribution, and lower panel displays methylation levels in CpG (blue), CHG (red), and CHH (green) contexts. (D) DNA methylation levels along gene regions, including 2-kb upstream, gene body, and 2-kb downstream regions in different sequence contexts (CpG, CHG, and CHH). (E) Relationship between gene expression and methylation levels in CpG, CHG, and CHH contexts. Genes were categorized into six expression ranks from lowest to highest expression, and corresponding methylation levels were plotted across upstream, gene body, and downstream regions.

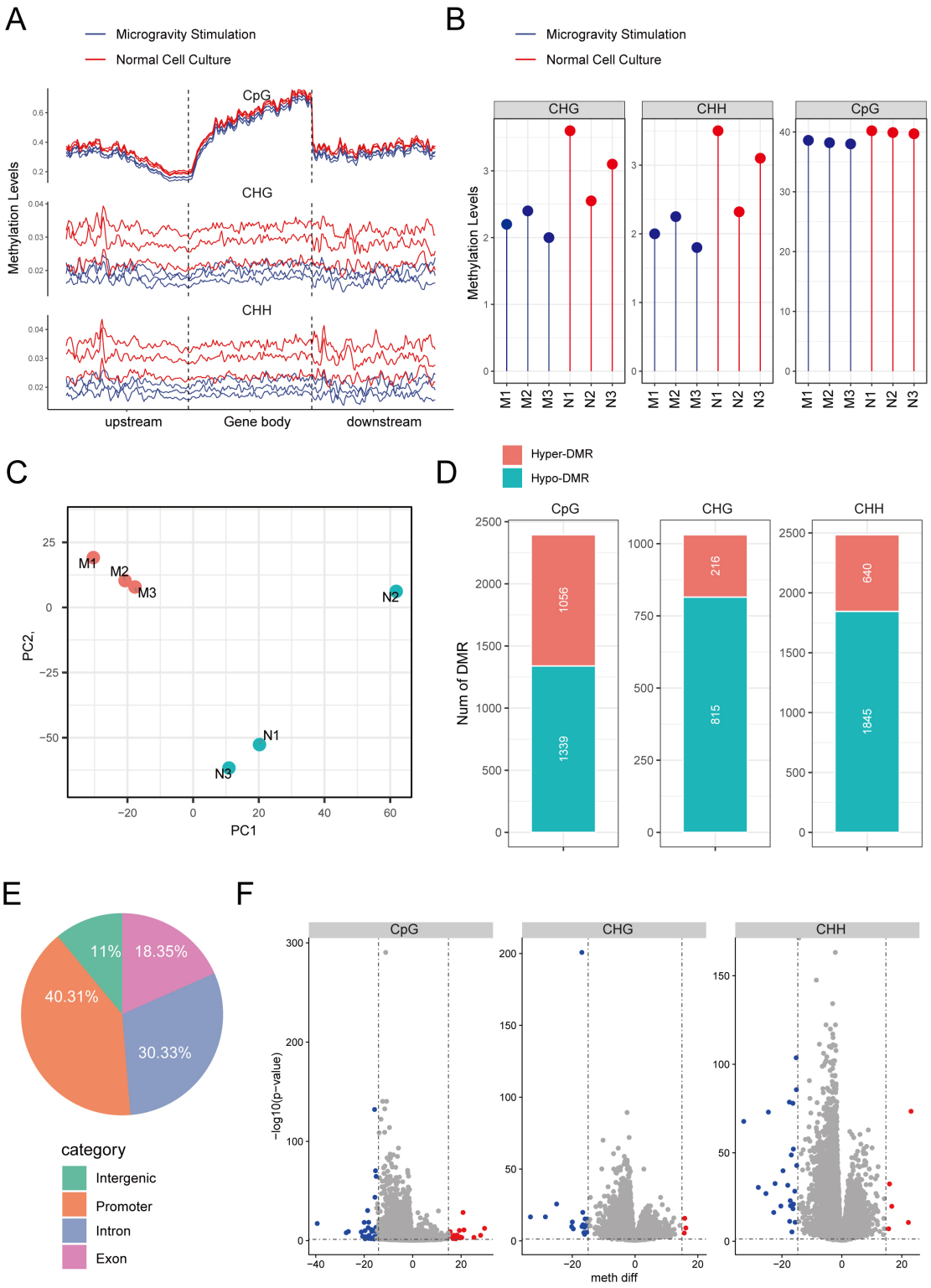

Fig. 3. DNA methylation pattern alterations in MC3T3-E1 cells under microgravity conditions. (A) Comparison of methylation levels in CpG, CHG, and CHH contexts between microgravity (M) and normal gravity groups (N). (B) Quantitative analysis of methylation level differences between groups. (C) Principal component analysis (PCA) of genome-wide methylation patterns showing distinct clustering between microgravity and normal gravity groups. (D) Distribution of differential methylation regions (DMRs) showing the number of hypomethylated (hypo) and hypermethylated (hyper) windows in CpG, CHG, and CHH contexts under microgravity conditions. (E) Genomic distribution of differential methylation windows across functional regions (promoter, exon, intron, and intergenic regions). (F) Methylation difference analysis in promoter regions across CpG, CHG, and CHH contexts, showing the distribution of methylation changes between microgravity and normal gravity conditions.

(Fig. 3A). Fig. 3B quantifies the differences in methylation levels across different groups. Based on the distribution of window methylation data, principal component analysis (PCA) showed a significant difference between the microgravity group and the normal group (Fig. 3C). In Fig. 3D, the differential methylation window (DMR) analysis revealed 1339 low methylation windows (hypo) and 1056 high methylation windows (hyper) in the CpG context; in the CHG context, there were 815 hypo and 216 hyper windows; and in the CHH context, 1845 hypo and 640 hyper windows. Overall, microgravity stimulation resulted in a notable increase in the number of low-methylation regions compared to high-methylation regions.

Next, we annotated the differential methylation windows, revealing that the promoter region accounted for 40.31%, exons for 18.35%, introns for 30.33%, and intergenic regions for 11% (Fig. 3E). Given that the methylation levels in the promoter region may significantly impact gene expression, we further analyzed the methylation status of the promoter regions. The results indicated that the number of high methylation windows (hyper) was 30, while the number of low methylation windows (hypo) was 89, with an impressive 56,245 windows showing no significant change (NS). Fig. 3F illustrates the methylation differences in the promoter regions across different contexts (CpG, CHG, CHH), highlighting that significant methylation changes in the CpG context are concentrated in regions with negative methylation differences. Collectively, these results suggest that microgravity stimulation significantly alters methylation patterns, potentially regulating gene expression through its effects on promoter region methylation levels.

Integrated Methylation Levels and Transcriptome Under Microgravity Stimulus

We performed a correlation analysis between genome-wide methylation and transcriptome levels under microgravity. The PCA revealed significant differences in gene expression between the microgravity (M) and normal gravity (N) groups (Fig. 4A). Differential expression analysis identified 2697 upregulated and 3172 downregulated genes, which were significantly enriched in apoptosis and ER stress pathways (Fig. 4B). Fig. 4C illustrates the significant downregulation of genes associated with DNA methylation in the microgravity group. Further qPCR and western blot analyses confirmed that under microgravity conditions, Dnmt3a exhibited the most pronounced downregulation, with its mRNA level decreasing by approximately 48% ($p < 0.001$) and protein level reduced by about 34% ($p < 0.05$) (Fig. 4D–F). To identify functional gene-methylation interactions, we integrated the RNA-seq and RRBS data based on genomic coordinates. We applied strict filtering criteria to identify high-confidence targets: (1) genes must be significantly differentially expressed (adjusted p-value $<$ 0.05); (2) genes must contain significant DMRs within their promoter regions (defined as 2 kb upstream of the transcription start site) with a methylation difference greater than 15% and an adjusted p-value < 0.05; and (3) genes must exhibit an inverse correlation between promoter methylation and expression levels. Based on this comprehensive screening, we identified eight candidate genes (listed in **Supplementary Table 4**). Among them, six genes showed reduced promoter methylation and upregulated expression: 9330188P03Rik, Iah1, Ddit3, Marcksl1, Slc22a23, and Dusp18. Notably, Ddit3 exhibited the most substantial upregulation (log2FoldChange >1) coupled with a ~20% decrease in promoter methylation. Conversely, two genes, Rprd1a and Igf2r, exhibited increased promoter methylation ($>20\%$ difference) accompanied by downregulated expression (Fig. 4G). We focused on the Ddit3 gene because it may play a significant role in both ER stress and apoptosis pathways (Fig. 4H). The functionality of this gene is closely related to cellular stress responses under microgravity conditions, suggesting its potential importance in regulating cell fate in such environments.

Effect of Dnmt3a in Microgravity-Induced Apoptosis of Osteoblasts

To investigate the effect of changes in Dnmt3a expression on the microgravity-induced osteoblast apoptosis model, we first assessed the efficiency of plasmid-mediated Dnmt3a overexpression by PCR. The results showed that the plasmid overexpressing Dnmt3a successfully increased Dnmt3a expression in microgravity-treated osteoblasts ($p < 0.05$) (Fig. 5A). Next, we analyzed the expression of apoptosis-related proteins by WB. The WB results revealed that Dnmt3a overexpression significantly suppressed the microgravity-induced alterations in apoptosis markers, reducing Bax expression by 35% ($p < 0.05$) and increasing Bcl-2 expression by 103% ($p < 0.05$) compared with the microgravity group (Fig. 5B,C), indicating that overexpression of Dnmt3a effectively attenuates the pro-apoptotic effect of microgravity on osteoblasts. Furthermore, CCK-8 assay results showed that Dnmt3a overexpression partially restored the inhibitory effect of microgravity on cell proliferation, elevating cell viability by 31% ($p < 0.001$) (Fig. 5D). Additionally, we evaluated the efficiency of siRNA-mediated knockdown of Dnmt3a by PCR, and the results showed that siRNA effectively reduced Dnmt3a expression ($p < 0.001$) (Fig. 5E). We selected Si-Dnmt3a-1 for the subsequent experiments. Flow cytometry analysis revealed that Dnmt3a inhibition significantly exacerbated the apoptosis rate in microgravity-treated cells, increasing apoptosis by 71% ($p < 0.01$) compared with the microgravity group (Fig. 5F,G), and WB further confirmed that Dnmt3a inhibition led to an increase in Bax and Cleaved-caspase-3 expression levels, with Bax expression increased by 37% ($p < 0.001$) and Cleaved-caspase-3 expression increased by 26% ($p < 0.05$), compared with the microgravity group, suggesting that Dnmt3a suppression enhances

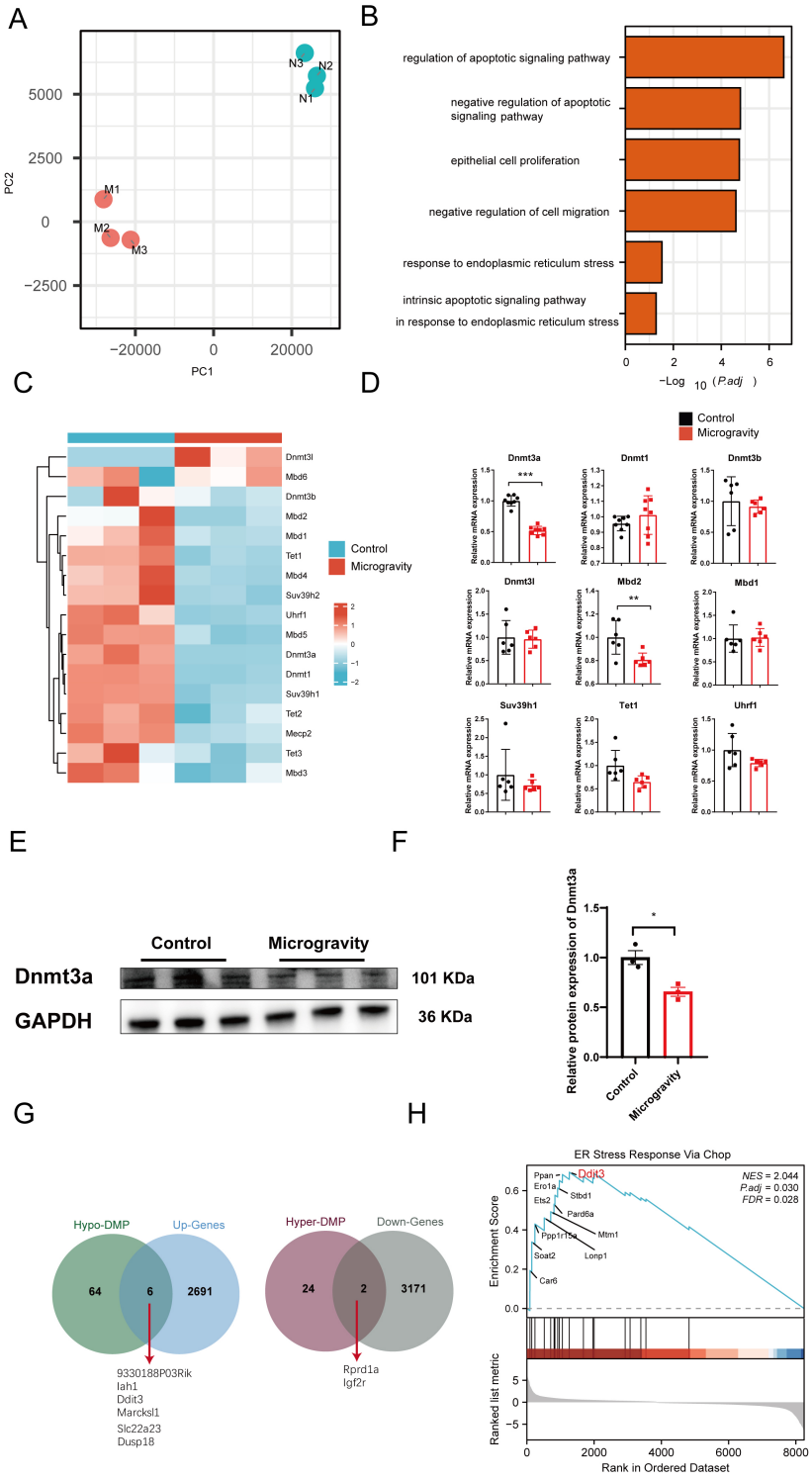

Fig. 4. Transcriptomic and methylation analysis under microgravity conditions. (A) Principal component analysis (PCA) of gene expression profiles between microgravity (M) and normal gravity (N) groups. (B) GO terms and KEGG pathway enrichment analysis of differentially expressed genes under microgravity conditions, showing significant enrichment in apoptosis and ER stress-related pathways. (C) Heatmap showing the expression patterns of DNA methylation-related genes under microgravity conditions. (D) Quantitative PCR validation of DNA methyltransferase expression changes, highlighting significant downregulation of Dnmt3a. (E,F) Confirmation of Dnmt3a downregulation by Western blot. (G) Correlation analysis between differential methylation promoters (DMPs) and differentially expressed genes (DEGs), identifying key genes with inverse correlation between promoter methylation and expression levels. (H) Gene Set Enrichment Analysis (GSEA) showing enriched pathways ranked by logFC and core genes contributing to the enrichment, with particular focus on apoptosis and ER stress pathways. Data shown as mean ± SD (n ≥ 3), *$p < 0.05$; **$p < 0.01$; ***$p < 0.001$.

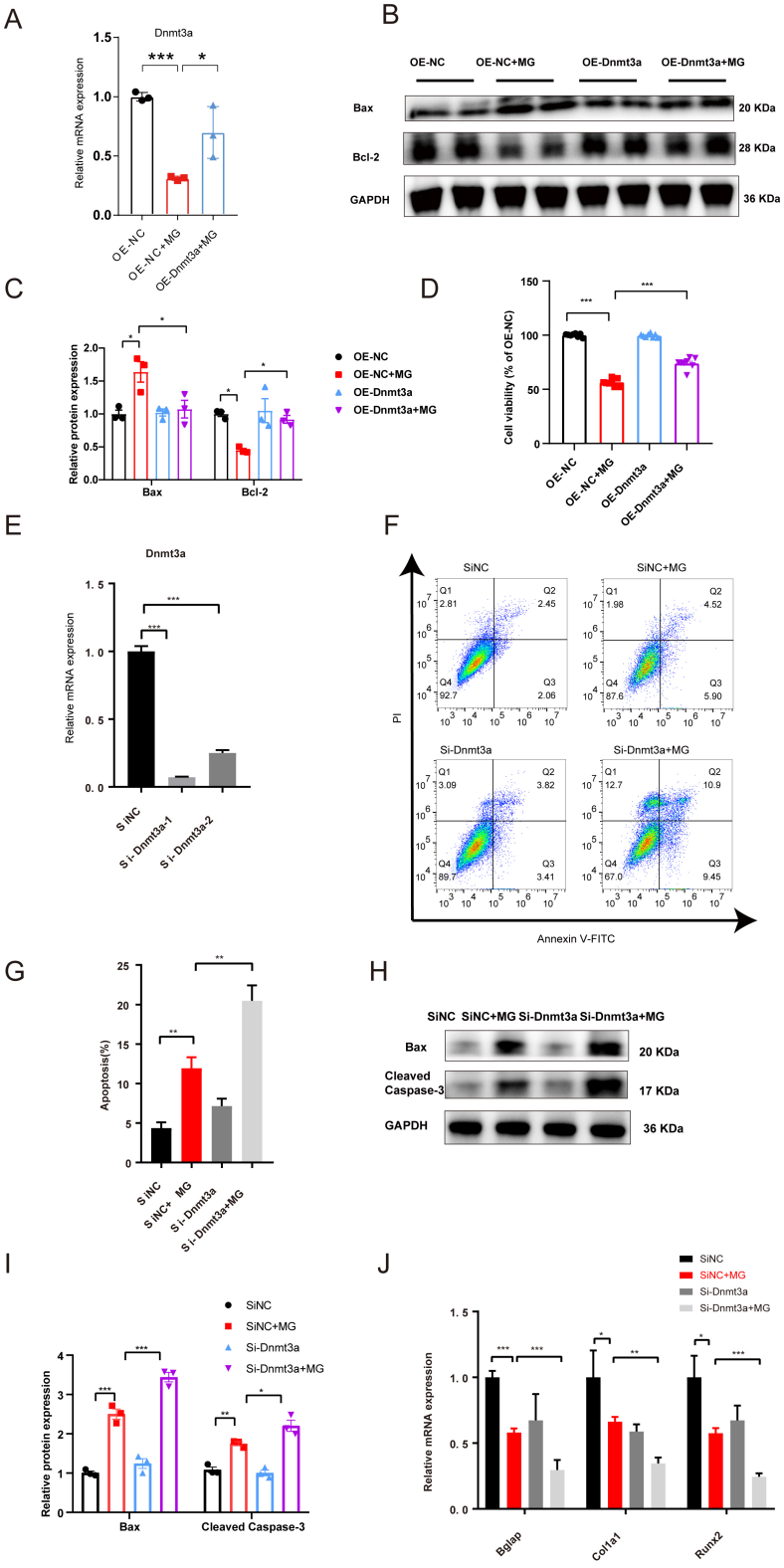

Fig. 5. Effect of Dnmt3a overexpression and knockdown on microgravity-induced osteoblast apoptosis. (A) PCR assessment of Dnmt3a overexpression efficiency. (B,C) WB analysis of apoptosis markers (Bax, Bcl-2) in microgravity-treated osteoblasts with Dnmt3a overexpression. (D) CCK-8 assay showing the effect of Dnmt3a overexpression on cell proliferation under microgravity. (E) PCR assessment of Dnmt3a knockdown efficiency. (F,G) Flow cytometry analysis of cell apoptosis in microgravity-treated osteoblasts with Dnmt3a knockdown. (H,I) WB analysis of apoptosis markers (Bax, Cleaved-caspase3) after Dnmt3a knockdown. (J) PCR analysis of osteoblast matrix protein gene expression (*Bglap*, *Col1a1*, *Runx2*) following Dnmt3a knockdown under microgravity. Microgravity (MG). Data shown as mean ± SD (n ≥ 3), *$p < 0.05$; **$p < 0.01$; ***$p < 0.001$.

the pro-apoptotic effect of microgravity (Fig. 5H,I). Moreover, PCR results showed that inhibiting Dnmt3a expression exacerbated the suppressive effect of microgravity on osteoblast matrix protein gene expression. Compared with the microgravity group, Dnmt3a inhibition led to a 49% reduction ($p < 0.001$) in *Bglap*, a 48% decrease ($p < 0.01$) in *Col1a1*, and a 57% decrease ($p < 0.001$) in *Runx2* expression, particularly affecting these key osteogenic genes (Fig. 5J). These findings indicate that Dnmt3a expression significantly affects osteoblast gene expression and proliferation, and its regulatory role under microgravity conditions is particularly important. In summary, overexpression of Dnmt3a can inhibit the pro-apoptotic effect of microgravity on osteoblasts and mitigate the suppression of cell proliferation induced by microgravity, while inhibition of Dnmt3a expression exacerbates these phenotypic effects.

Ddit3 in Osteoblast is an Important Downstream Target Regulated by Dnmt3a

Based on bioinformatics analysis, Ddit3 was found to exhibit promoter region hypomethylation and increased expression under microgravity conditions (Fig. 4G). To investigate whether Ddit3 serves as a downstream target regulated by Dnmt3a, we performed MSP analysis, which confirmed that compared with the control group, microgravity induces demethylation of the Ddit3 promoter region in osteoblasts, showing a 45% reduction ($p < 0.01$) in promoter methylation (Fig. 6A). This finding was further validated by BSP analysis, which revealed a significant reduction in Ddit3 promoter region methylation levels under microgravity, showing a 62% decrease ($p < 0.001$) in promoter methylation (Fig. 6B,C). Importantly, microgravity also promoted the upregulation of Ddit3 gene expression ($p < 0.001$) (Fig. 6D). These results suggest that Ddit3 expression is regulated by its methylation status. To determine the role of Dnmt3a in Ddit3 promoter region methylation, we conducted further experiments under conditions of Dnmt3a inhibition. MSP analysis showed that suppressing Dnmt3a expression led to a further reduction in Ddit3 promoter region methylation levels ($p < 0.001$) (Fig. 6E), and PCR results demonstrated a concomitant increase in Ddit3 gene expression ($p < 0.001$) (Fig. 6F). These findings indicate that Dnmt3a regulates Ddit3 expression through methylation. To evaluate the function of Ddit3, we performed siRNA-mediated knockdown of Ddit3 and selected Si-Ddit3-1 for the subsequent experiments (Fig. 6G). PCR and flow cytometry analyses were performed. The results showed that inhibition of Ddit3 under microgravity conditions restored the expression of osteogenic genes, including *Bglap* ($p < 0.001$), *Runx2* ($p < 0.01$), and *Col1a1* ($p < 0.01$) (Fig. 6H), and significantly attenuated microgravity-induced osteoblast apoptosis ($p < 0.01$) (Fig. 6I). Notably, under microgravity conditions, combined inhibition of Dnmt3a and Ddit3 partially restored the expression of osteogenic genes compared with Dnmt3a inhibition alone (Fig. 6H). Consistently, additional suppression of Ddit3 in Dnmt3a-inhibited osteoblasts led to a 58% reduction in apoptosis relative to cells with Dnmt3a suppression alone ($p < 0.001$) (Fig. 6I). These findings indicate that the regulatory role of Dnmt3a in osteoblast phenotype is, at least in part, mediated through Ddit3.

The Regulatory Effect of Ddit3 on Osteoblast Phenotype is Dependent on ER Stress

To investigate the mechanism through which Ddit3 exerts its effects under microgravity conditions, we first examined changes in the ER stress pathway associated with Ddit3 (Fig. 4H). WB analysis revealed that microgravity markedly induced the expression of ER stress–related proteins, with p-PERK, p-IRE1α, and XBP1s upregulated by 3.2- ($p < 0.001$), 2.1- ($p < 0.001$), and 3.8-fold ($p < 0.001$), respectively (Fig. 7A,B), indicating robust activation of the ER stress pathway under microgravity conditions. Further experiments demonstrated that inhibiting Ddit3 expression effectively alleviated the ER stress response induced by microgravity. Compared with the microgravity group, Ddit3 inhibition significantly reduced p-PERK, p-IRE1α, and XBP1s levels by 57% ($p < 0.001$), 48% ($p < 0.001$), and 56% ($p < 0.001$), respectively, highlighting the critical role of Ddit3 in regulating ER stress (Fig. 7A,B). To further verify the role of the ER stress pathway under microgravity conditions, we used the ER stress inhibitor 4PBA for intervention. The results showed that 4PBA effectively reversed the microgravity-induced ER stress response ($p < 0.001$) (Fig. 7C,D). In addition, under microgravity conditions, 4PBA significantly alleviated the inhibitory effect of Dnmt3a knockdown on the expression of osteogenic genes such as *Bglap* ($p < 0.01$), *Col1a1* ($p < 0.001$), and *Runx2* ($p < 0.001$) (Fig. 7E,F). These findings suggest that under microgravity conditions, Ddit3 regulates osteoblast phenotype by modulating the ER stress pathway.

Ddit3 Knockdown Prevents Tail Suspension (TS)-Induced Bone Loss In Vivo

To investigate the regulatory role of Ddit3 in osteoporosis, we employed a TS mouse model to simulate weightlessness-induced osteoporosis. We injected AAV2 vectors carrying Ddit3 shRNA or ShNC into the femoral distal surface to knock down Ddit3 gene expression and assess its effect on TS-induced osteoporotic phenotypes. PCR results confirmed that AAV2 successfully knocked down Ddit3 expression ($p < 0.001$) (Fig. 8B).

Micro-CT analysis revealed that the TS group exhibited significant osteoporotic characteristics, including decreased bone mineral density (BMD) ($p < 0.001$), trabecular bone volume/total volume ratio (BV/TV) ($p < 0.001$), trabecular number (Tb.N) ($p < 0.01$), trabecular thickness (Tb.Th) ($p < 0.001$), and increased trabecular separation (Tb.Sp) ($p < 0.001$). In contrast, Ddit3 inhibition notably improved these osteoporotic parameters (Fig. 8A,C).

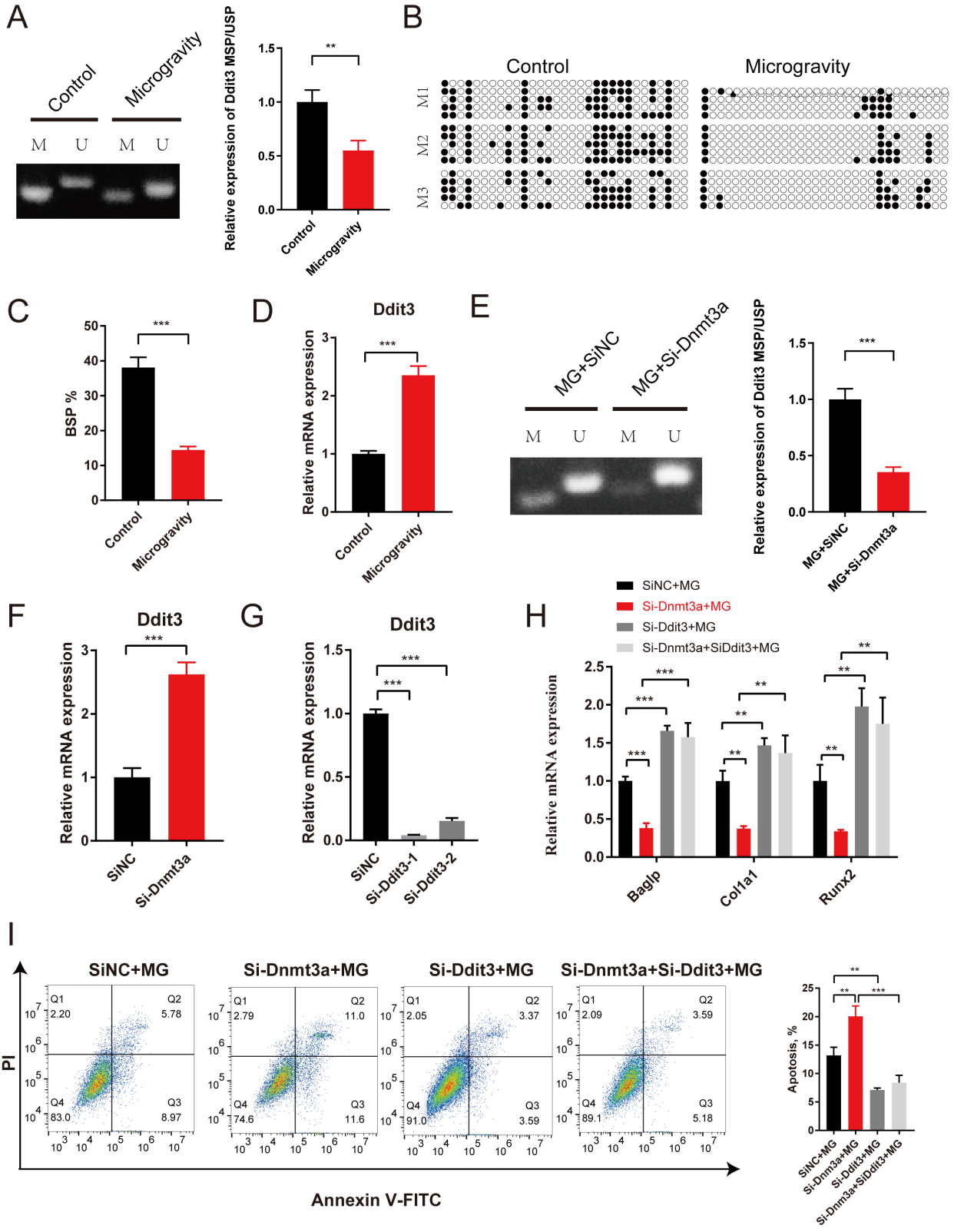

Fig. 6. Experimental validation of Ddit3 as a downstream target of Dnmt3a under microgravity conditions. (A) MSP analysis of Ddit3 promoter region demethylation in microgravity. (B,C) BSP analysis of Ddit3 promoter region methylation under microgravity. (D) PCR analysis of Ddit3 expression in microgravity. (E) MSP analysis of Ddit3 promoter region methylation following Dnmt3a inhibition. (F) PCR analysis of Ddit3 expression after Dnmt3a inhibition. (G,H) PCR analysis of Ddit3 and osteogenic gene expression (*Bglap*, *Runx2*, *Col1a1*) upon Ddit3 inhibition. (I) Flow cytometry analysis of osteoblast apoptosis following Ddit3 inhibition in microgravity. Data shown as mean ± SD (n ≥ 3), $^{**}p < 0.01$; $^{***}p < 0.001$.

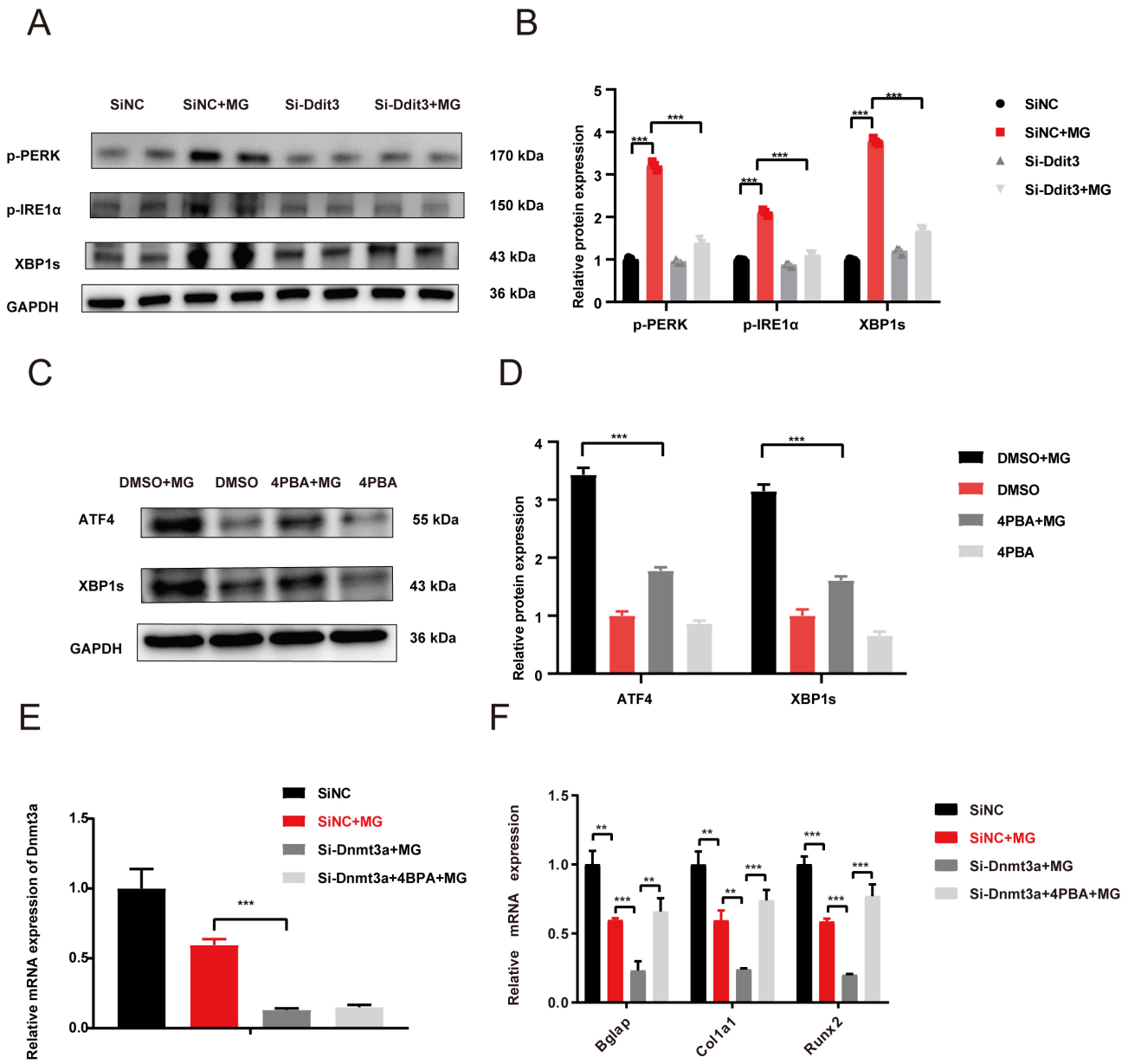

Fig. 7. Verification of the ER stress pathway modulation by Ddit3 under microgravity. (A,B) WB analysis to detect ER stress-related proteins (p-PERK, p-IRE1α, and XBP1s) under microgravity. (C,D) WB analysis to evaluate the effect of the ER stress inhibitor 4PBA on microgravity-induced ER stress. (E) PCR analysis of Dnmt3a mRNA expression following 4PBA treatment under microgravity. (F) PCR analysis of osteogenic gene expression (*Bglap*, *Col1a1*, *Runx2*) following 4PBA treatment under microgravity. Data shown as the mean $\pm$ SD (n $\geq$ 3), $^{**}p < 0.01$; $^{***}p < 0.001$.

Further immunohistochemical analysis showed that inhibiting Ddit3 significantly increased OCN expression in the TS group compared with the ShNC-treated TS group ($p < 0.01$) (Fig. 8D), suggesting enhanced osteogenic capacity. Consistent with this finding, Masson staining indicated that Ddit3 suppression partially restored bone structural integrity disrupted by TS (Fig. 8E). HE staining further confirmed that inhibition of Ddit3 effectively alleviated the TS-induced osteoporotic phenotype, as evidenced by improved trabecular morphology and overall bone architecture (Fig. 8F). These results demonstrate that Ddit3 knockdown exerts a protective effect against TS-induced osteoporosis, highlighting its potential as a therapeutic target for bone protection.

Discussion

Osteoporosis is a common systemic skeletal disease, which severely impacts the quality of life of affected individuals. It is projected that by 2030, the prevalence of osteoporosis among adults aged 50 and above will reach 13.6% [31]. The pathogenesis of osteoporosis is highly

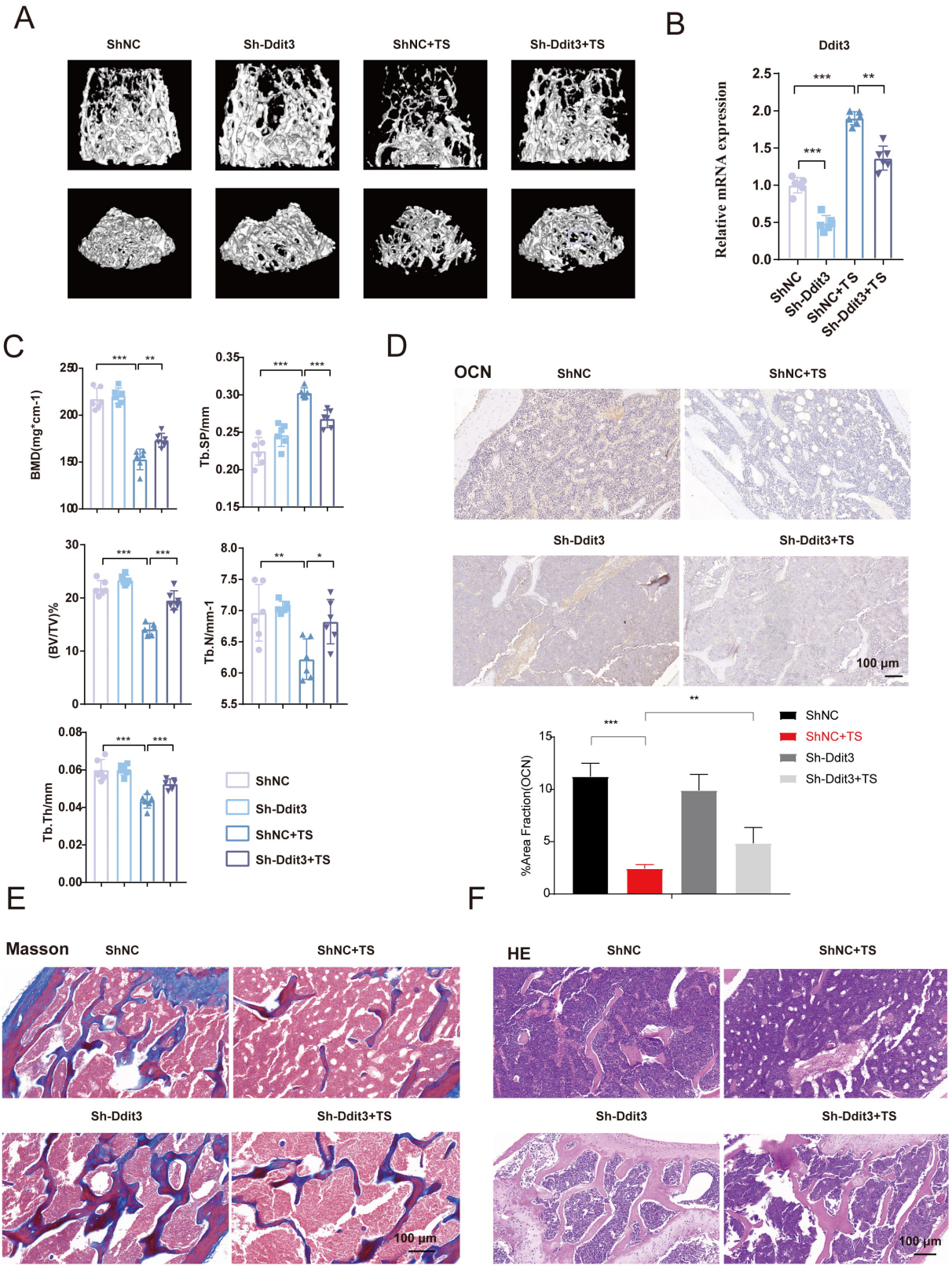

Fig. 8. Effects of Ddit3 inhibition on osteoporosis in the TS mouse model. (A) Representative images from Micro-CT analysis. (B) PCR verification of Ddit3 knockdown efficiency. (C) Micro-CT analysis of bone mineral density (BMD), trabecular bone volume (BV/TV), trabecular number (Tb.N), trabecular thickness (Tb.Th), and trabecular separation (Tb.Sp) in different groups. (D) IHC analysis of OCN expression. (E) Masson staining to evaluate bone integrity. (F) HE staining to assess bone structure. Data shown as the mean ± SD (n ≥ 3), *$p < 0.05$; **$p < 0.01$; ***$p < 0.001$. scale bar: 100 μm.

complex, with key risk factors including hormonal changes, genetic factors, and mechanical environmental alterations [32,33]. Among these, changes in the mechanical environment are the primary exogenous factor [34]. It is widely recognized that the mechanical environment is critical for bone homeostasis and fracture healing [35]. Microgravity has been shown to significantly reduce bone mass, accompanied by significant changes in bone microstructure [36,37]. With the increasing development of space exploration, preventing microgravity-induced damage to bones is crucial for bone protection. From a cellular biology perspective, microgravity has been demonstrated to induce significant changes in cell behavior, including disturbances in osteoblast differentiation and altered activity [38,39]. This phenomenon is partially attributed to the dysregulation of epigenetic mechanisms, including m6A RNA methylation [40] and histone modifications [15]. Therefore, exploring the epigenetic regulatory mechanisms driving microgravity-induced osteoporosis is critical for the rational identification of bone-protective therapeutic targets.

In this study, we report several novel findings that contribute to the understanding of the epigenetic mechanisms underlying osteoporosis under microgravity conditions. We found that microgravity induces an apoptotic phenotype in osteoblasts and suppresses their cell activity, consistent with previous studies [10,41]. Further investigations revealed that microgravity significantly affects the methylation status of osteoblasts, with notable changes in CpG methylation levels. DNA methylation at CpG islands in the promoter regions leads to silencing of downstream genes, while enhancer methylation may be associated with either a decrease or increase in gene expression [42]. This suggests that DNA methylation-regulated gene alterations may play a key molecular role in microgravity-induced cell apoptosis. To identify the specific molecules regulating DNA methylation modifications, we performed transcriptomic data analysis on the microgravity-treated group. Pathway enrichment analysis revealed that differentially expressed genes were primarily associated with cell apoptosis, proliferation, and the ER stress pathway. This further confirmed that microgravity can indeed induce osteoblast apoptosis. Importantly, we found that Dnmt3a, Dnmt1, and Dnmt3b, which are related to DNA methylation modification, were significantly downregulated in the microgravity group. PCR and Western blot results corroborated the findings that both the gene and protein levels of Dnmt3a were consistently decreased under microgravity conditions.

Dnmt3a is a key enzyme mediating de novo DNA methylation, thereby affecting the transcriptional landscape of various genes, including those involved in apoptotic responses [22,24]. Studies have shown that Dnmt3a promotes osteoblast differentiation and prevents postmenopausal osteoporosis by regulating the PPARγ/SCD1/GLUT1 axis [21]. Additionally, mutations in Dnmt3a mediate increased osteoclast activity [43]. These findings suggest that Dnmt3a may play a protective role in osteoporosis. Given that Dnmt3a is involved in the regulation of apoptotic responses, we combined the methylation data with the transcriptomic data to identify genes with a low methylation status and high expression, including Iah1, Ddit3, Marcksl1, Slc22a23, aDusp18, and 9330188P03Rik. Notably, we found that Ddit3 is associated with apoptotic pathway responses. To confirm the role of Dnmt3a in microgravity-induced osteoblast apoptosis, we explored and found that overexpression of Dnmt3a alleviated microgravity-induced osteoblast apoptosis, while knockdown of Dnmt3a exacerbated the apoptotic phenotype and inhibited osteoblast activity. These results indicate that Dnmt3a helps maintain osteoblast activity under microgravity conditions. Furthermore, as Ddit3 was found to be hypomethylated and upregulated in the microgravity group, we investigated whether Dnmt3a mediates the methylation modification of Ddit3. Combining MSP and BSP experiments, we observed that Ddit3 is hypomethylated in the microgravity group, and its gene expression level is elevated. Importantly, when Dnmt3a expression was suppressed, Ddit3's methylation status was further reduced. Moreover, inhibition of Dnmt3a promoted Ddit3 expression.

Importantly, inhibition of Ddit3 expression could reverse the effects of Dnmt3a knockdown on microgravity-induced osteoblast apoptosis. This suggests that, under microgravity conditions, the regulatory effect of Dnmt3a on osteoblast phenotype is partially dependent on its regulation of Ddit3. Recent studies have shown that Ddit3 can promote LPS-induced osteoblast apoptosis by inhibiting mitochondrial autophagy [44]. Additionally, inhibition of Ddit3 has been shown to benefit bone remodeling [45]. These findings further support the critical role of Ddit3 in microgravity-induced cell apoptosis. Since Ddit3 is associated with the ER stress pathway [46], we investigated its role in osteoblast phenotype changes related to ER stress under microgravity conditions. The results demonstrated that inhibiting Ddit3 significantly reversed the activation of the ER stress signaling pathway induced by microgravity. Moreover, the ER stress inhibitor 4PBA effectively reversed the inhibitory effects of Dnmt3a knockdown on osteoblast activity under microgravity conditions. This indicates that, under microgravity conditions, the regulation of osteoblast phenotype by Dnmt3a is partially dependent on the Ddit3-related ER stress signaling pathway. Recent studies have also highlighted that inhibition of ER stress is a promising therapeutic target for osteoporosis [47]. Therefore, the Ddit3-associated ER stress signaling pathway may serve as a crucial target for inhibiting cell apoptosis. To further analyze the role of Ddit3, we used AAV2 virus to suppress Ddit3 expression *in vivo*. The results showed that inhibition of Ddit3 effectively alleviated the osteoporosis phenotype induced by TS. This confirms that the Ddit3-related ER stress pathway may be a potential target for treating osteoporosis under microgravity conditions.

Conclusion

Therefore, our findings demonstrate that under microgravity conditions, the downregulation of Dnmt3a results in hypomethylation of the Ddit3 promoter, which subsequently activates ER stress and induces osteoblast apoptosis, ultimately promoting the development of osteoporosis. Collectively, this study elucidates a distinct epigenetic regulatory mechanism underlying microgravity-induced osteoporosis and provides compelling experimental evidence for identifying potential therapeutic targets within the Dnmt3a–Ddit3 signaling axis.

However, despite the preliminary evidence provided in this study regarding the regulatory roles of Dnmt3a and Ddit3 in osteoblast function under microgravity conditions, several limitations remain. First, our study primarily relied on rotational simulated microgravity for *in vitro* experiments and a tail-suspension mouse model for *in vivo* analysis. Although these models are widely used and provide valuable insights, the rotational culture system only mimics reduced mechanical loading through a low-shear, random-orientation environment, and cannot fully reproduce the absence of gravitational vectors or cosmic radiation observed in true spaceflight. Similarly, the tail-suspension model, while effectively simulating skeletal unloading under microgravity, introduces physiological stresses such as altered circulation, muscle atrophy, and metabolic changes, which may confound bone remodeling processes. Future research should therefore employ more complex and realistic microgravity models, including space experiments, as well as clinical samples, to validate our conclusions. Second, the present study employed young mice at a specific skeletal stage. Future studies are warranted to systematically evaluate the effects of tail suspension on bone loss across different age groups, in order to elucidate potential age-dependent differences in susceptibility and disease progression. Third, the exact molecular mechanisms by which Ddit3 contributes to microgravity-induced osteoporosis have not been fully elucidated. Future studies could explore the interactions between Ddit3 and other upstream or downstream signaling pathways of the ER stress response. Additionally, further investigation is needed to determine how the Dnmt3a–Ddit3 axis could be targeted for therapeutic interventions and to develop effective treatment strategies.

Availability of Data and Materials

The datasets generated and/or analyzed during the current study are available from the corresponding author upon reasonable request.

Author Contributions

CS: Writing—original draft, Resources, Software, Investigation, Data curation, Formal analysis, Conceptualization, Funding acquisition. FT: Writing—original draft, Visualization, Methodology, Supervision, Project administration, Conceptualization, Funding acquisition. YX: Writing—review & editing, Validation, Methodology, Investigation, Data curation, Conceptualization, Funding acquisition. All authors read and approved the final manuscript and agreed to be accountable for all aspects of the work.

Ethics Approval and Consent to Participate

The study was approved by the Experimental Animal Ethics Committee of The Second Hospital of Lanzhou University (No. D2024-685).

Acknowledgment

Not applicable.

Funding

This work was supported by The National Natural Science Foundation of China (82060405 and 82360436); Lanzhou Science and Technology Plan Program (2021-RC-102); Natural Science Foundation of Gansu Province (22JR5RA943, 22JR5RA956, 24YFFA043, and 23JRRA1500); Cuiying Scientific and Technological Innovation Program of Lanzhou University Second Hospital (CY2021-MS-A07, CY2022-MS-A19); Key Talents Program of Gansu Province (2025RCXM082).

Conflict of Interest

The authors declare no conflict of interest.

Supplementary Material

Supplementary material associated with this article can be found, in the online version, at https://doi.org/10.24976/Discov.Med.202638206.58.

References

[1] Foessl I, Dimai HP, Obermayer-Pietsch B. Long-term and sequential treatment for osteoporosis. Nature Reviews. Endocrinology. 2023; 19: 520–533. https://doi.org/10.1038/s41574-023-00866-9.

[2] Varacallo MA, Fox EJ. Osteoporosis and its complications. The Medical Clinics of North America. 2014; 98: 817–831, xii–xiii. https://doi.org/10.1016/j.mcna.2014.03.007.

[3] Porter JL, Varacallo MA. Osteoporosis. StatPearls: Treasure Island (FL). 2022.

[4] Greenstein AS, Gorczyca JT. Orthopedic Surgery and the Geriatric Patient. Clinics in Geriatric Medicine. 2019; 35: 65–92. https://doi.org/10.1016/j.cger.2018.08.007.

[5] Compston JE, McClung MR, Leslie WD. Osteoporosis. Lancet. 2019; 393: 364–376. https://doi.org/10.1016/S0140-6736(18)32112-3.

[6] Yamamoto Y, Chiba T, Dohmae S, Higashi K, Nakazawa A.

Osteoporosis medication after fracture in older adults: an administrative data analysis. Osteoporosis International. 2021; 32: 1245–1246. https://doi.org/10.1007/s00198-021-05973-9.

[7] Sözen T, Özışık L, Başaran NÇ. An overview and management of osteoporosis. European Journal of Rheumatology. 2017; 4: 46–56. https://doi.org/10.5152/eurjrheum.2016.048.

[8] Adejuyigbe B, Kallini J, Chiou D, Kallini JR. Osteoporosis: Molecular Pathology, Diagnostics, and Therapeutics. International Journal of Molecular Sciences. 2023; 24: 14583. https://doi.org/10.3390/ijms241914583.

[9] Smith JK. Osteoclasts and Microgravity. Life. 2020; 10: 207. https://doi.org/10.3390/life10090207.

[10] Wang Y, Wang K, Hu Z, Zhou H, Zhang L, Wang H, *et al*. MicroRNA-139-3p regulates osteoblast differentiation and apoptosis by targeting ELK1 and interacting with long noncoding RNA ODSM. Cell Death & Disease. 2018; 9: 1107. https://doi.org/10.1038/s41419-018-1153-1.

[11] Jie J, Li W, Wang G, Xu X. FK506 ameliorates osteoporosis caused by osteoblast apoptosis via suppressing the activated CaN/NFAT pathway during oxidative stress. Inflammation Research. 2021; 70: 789–797. https://doi.org/10.1007/s00011-021-01452-3.

[12] Deng S, Nie ZG, Peng PJ, Liu Y, Xing S, Long LS, *et al*. Decrease of GSK3β Ser-9 Phosphorylation Induced Osteoblast Apoptosis in Rat Osteoarthritis Model. Current Medical Science. 2019; 39: 75–80. https://doi.org/10.1007/s11596-019-2002-x.

[13] Zhong Y, Zhou X, Pan Z, Zhang J, Pan J. Role of epigenetic regulatory mechanisms in age-related bone homeostasis imbalance. FASEB Journal. 2024; 38: e23642. https://doi.org/10.1096/fj.202302665R.

[14] Xu F, Li W, Yang X, Na L, Chen L, Liu G. The Roles of Epigenetics Regulation in Bone Metabolism and Osteoporosis. Frontiers in Cell and Developmental Biology. 2021; 8: 619301. https://doi.org/10.3389/fcell.2020.619301.

[15] Gambacurta A, Merlini G, Ruggiero C, Diedenhofen G, Battista N, Bari M, *et al*. Human osteogenic differentiation in Space: proteomic and epigenetic clues to better understand osteoporosis. Scientific Reports. 2019; 9: 8343. https://doi.org/10.1038/s41598-019-44593-6.

[16] Zhang Z, Duan Y, Huo J. Lipid Metabolism, Methylation Aberrant, and Osteoporosis: A Multi-omics Study Based on Mendelian Randomization. Calcified Tissue International. 2024; 114: 147–156. https://doi.org/10.1007/s00223-023-01160-6.

[17] Mattei AL, Bailly N, Meissner A. DNA methylation: a historical perspective. Trends in Genetics. 2022; 38: 676–707. https://doi.org/10.1016/j.tig.2022.03.010.

[18] Dura M, Teissandier A, Armand M, Barau J, Lapoujade C, Fouchet P, *et al*. DNMT3A-dependent DNA methylation is required for spermatogonial stem cells to commit to spermatogenesis. Nature Genetics. 2022; 54: 469–480. https://doi.org/10.1038/s41588-022-01040-z.

[19] Khazaei S, Chen CCL, Andrade AF, Kabir N, Azarafshar P, Morcos SM, *et al*. Single substitution in H3.3G34 alters DNMT3A recruitment to cause progressive neurodegeneration. Cell. 2023; 186: 1162–1178.e20. https://doi.org/10.1016/j.cell.2023.02.023.

[20] Panach L, Pertusa C, Martínez-Rojas B, Acebrón Á, Mifsut D, Tarín JJ, *et al*. Comparative transcriptome analysis identifies CARM1 and DNMT3A as genes associated with osteoporosis. Scientific Reports. 2020; 10: 16298. https://doi.org/10.1038/s41598-020-72870-2.

[21] Lu L, Wang L, Wu J, Yang M, Chen B, Wang H, *et al*. *DNMT3a* promotes osteoblast differentiation and alleviates osteoporosis via the *PPARγ*/*SCD1*/*GLUT1* axis. Epigenomics. 2022; 14: 777–792. https://doi.org/10.2217/epi-2021-0391.

[22] Jing W, Song N, Liu YP, Qu XJ, Qi YF, Li C, *et al*. DNMT3a promotes proliferation by activating the STAT3 signaling pathway and depressing apoptosis in pancreatic cancer. Cancer Management and Research. 2019; 11: 6379–6396. https://doi.org/10.2147/CMAR.S201610.

[23] Sun J, Ji J, Huo G, Song Q, Zhang X. miR-182 induces cervical cancer cell apoptosis through inhibiting the expression of DNMT3a. International Journal of Clinical and Experimental Pathology. 2015; 8: 4755–4763.

[24] Lu W, Lu T, Wei X. Downregulation of DNMT3a expression increases miR-182-induced apoptosis of ovarian cancer through caspase-3 and caspase-9-mediated apoptosis and DNA damage response. Oncology Reports. 2016; 36: 3597–3604. https://doi.org/10.3892/or.2016.5134.

[25] Singh KP, Kumari R, Dumond JW. Simulated microgravity-induced epigenetic changes in human lymphocytes. Journal of Cellular Biochemistry. 2010; 111: 123–129. https://doi.org/10.1002/jcb.22674.

[26] Yang F, Chen C, Yang C, Chen R, Liu Z, Wen L, *et al*. Exosome-mediated perturbation of the immune-bone metabolism axis: a mechanistic investigation into bone loss in a simulated microgravity environment. Artificial Cells, Nanomedicine, and Biotechnology. 2025; 53: 494–513. https://doi.org/10.1080/21691401.2025.2576277.

[27] Krueger F, Andrews SR. Bismark: a flexible aligner and methylation caller for Bisulfite-Seq applications. Bioinformatics. 2011; 27: 1571–1572. https://doi.org/10.1093/bioinformatics/btr167.

[28] Zhou Q, Lim JQ, Sung WK, Li G. An integrated package for bisulfite DNA methylation data analysis with Indel-sensitive mapping. BMC Bioinformatics. 2019; 20: 47. https://doi.org/10.1186/s12859-018-2593-4.

[29] Akalin A, Kormaksson M, Li S, Garrett-Bakelman FE, Figueroa ME, Melnick A, *et al*. methylKit: a comprehensive R package for the analysis of genome-wide DNA methylation profiles. Genome Biology. 2012; 13: R87. https://doi.org/10.1186/gb-2012-13-10-r87.

[30] Huang X, Zhu Y, Sun S, Gao X, Yang Y, Xu H, *et al*. Exercise maintains bone homeostasis by promoting osteogenesis through STAT3. International Journal of Biological Sciences. 2023; 19: 2021–2033. https://doi.org/10.7150/ijbs.82744.

[31] Harris K, Zagar CA, Lawrence KV. Osteoporosis: Common Questions and Answers. American Family Physician. 2023; 107: 238–246.

[32] Vaishya R, Iyengar KP, Jain VK, Vaish A. Demystifying the Risk Factors and Preventive Measures for Osteoporosis. Indian Journal of Orthopaedics. 2023; 57: 94–104. https://doi.org/10.1007/s43465-023-00998-0.

[33] Arjunan D, Prasad TN, Das L, Bhadada SK. Osteoporosis and Obesity. Indian Journal of Orthopaedics. 2023; 57: 218–224. https://doi.org/10.1007/s43465-023-01052-9.

[34] Coulombe JC, Senwar B, Ferguson VL. Spaceflight-Induced Bone Tissue Changes that Affect Bone Quality and Increase Fracture Risk. Current Osteoporosis Reports. 2020; 18: 1–12. https://doi.org/10.1007/s11914-019-00540-y.

[35] Wähnert D, Greiner J, Brianza S, Kaltschmidt C, Vordemvenne T, Kaltschmidt B. Strategies to Improve Bone Healing: Innovative Surgical Implants Meet Nano-/Micro-Topography of Bone Scaffolds. Biomedicines. 2021; 9: 746. https://doi.org/10.3390/biomedicines9070746.

[36] Hu Y, Tian H, Chen W, Liu Y, Cao Y, Pei H, *et al*. The Critical Role of The Piezo1/β-catenin/ATF4 Axis on The Stemness of Gli1$^+$ BMSCs During Simulated Microgravity-Induced Bone Loss. Advanced Science. 2023; 10: e2303375. https://doi.org/10.1002/advs.202303375.

[37] Montagna G, Pani G, Flinkman D, Cristofaro F, Pascucci B, Massimino L, *et al*. Long-term osteogenic differentiation of hu-

man bone marrow stromal cells in simulated microgravity: novel proteins sighted. Cellular and Molecular Life Sciences. 2022; 79: 536. https://doi.org/10.1007/s00018-022-04553-2.

[38] Fan C, Wu Z, Cooper DML, Magnus A, Harrison K, Eames BF, *et al*. Activation of Focal Adhesion Kinase Restores Simulated Microgravity-Induced Inhibition of Osteoblast Differentiation via Wnt/B-Catenin Pathway. International Journal of Molecular Sciences. 2022; 23: 5593. https://doi.org/10.3390/ijms23105593.

[39] Liu J, Leng FF, Gao YH, He WF, Wang JF, Xian CJ, *et al*. Protection of primary cilia is an effective countermeasure against the impairment of osteoblast function induced by simulated microgravity. Journal of Cellular and Molecular Medicine. 2023; 27: 36–51. https://doi.org/10.1111/jcmm.17628.

[40] Sun Q, Xu L, Hu Z, Liu J, Yu T, Li M, *et al*. Melatonin Regulates Osteoblast Differentiation through the m6A Reader hnRNPA2B1 under Simulated Microgravity. Current Issues in Molecular Biology. 2024; 46: 9624–9638. https://doi.org/10.3390/cimb46090572.

[41] Xu L, Zhang X, Li G, Zhang L, Zhang S, Shi F, *et al*. Inhibition of SIRT1 by miR-138-5p provides a mechanism for inhibiting osteoblast proliferation and promoting apoptosis under simulated microgravity. Life Sciences in Space Research. 2023; 36: 59–69. https://doi.org/10.1016/j.lssr.2022.08.001.

[42] Hattori N, Liu YY, Ushijima T. DNA Methylation Analysis. Methods in Molecular Biology. 2023; 2691: 165–183. https://doi.org/10.1007/978-1-0716-3331-1_13.

[43] Kim PG, Niroula A, Shkolnik V, McConkey M, Lin AE, Słabicki M, *et al*. Dnmt3a-mutated clonal hematopoiesis promotes osteoporosis. The Journal of Experimental Medicine. 2021; 218: e20211872. https://doi.org/10.1084/jem.20211872.

[44] Dong Z, Yang B, Jia M, Yang C, Wang S, Mu H, *et al*. DDIT3/CHOP promotes LPS/ATP-induced pyroptosis in osteoblasts via mitophagy inhibition. Biochimica et Biophysica Acta. Molecular Cell Research. 2024; 1871: 119712. https://doi.org/10.1016/j.bbamcr.2024.119712.

[45] Jia M, Dong Z, Dong W, Yang B, He Y, Wang Y, *et al*. DDIT3 deficiency accelerates bone remodeling during bone healing by enhancing osteoblast and osteoclast differentiation through ULK1-mediated autophagy. Bone. 2024; 182: 117058. https://doi.org/10.1016/j.bone.2024.117058.

[46] Yong J, Parekh VS, Reilly SM, Nayak J, Chen Z, Lebeaupin C, *et al*. *Chop*/*Ddit3* depletion in β cells alleviates ER stress and corrects hepatic steatosis in mice. Science Translational Medicine. 2021; 13: eaba9796. https://doi.org/10.1126/scitranslmed.aba9796.

[47] Zhong M, Wu Z, Chen Z, Ren Q, Zhou J. Advances in the interaction between endoplasmic reticulum stress and osteoporosis. Biomedicine & Pharmacotherapy. 2023; 165: 115134. https://doi.org/10.1016/j.biopha.2023.115134.